WILEY-VCH

DOI: 10.1002/ ((please add manuscript number))
Article type: Full Paper

In-situ TEM study of volume expansion in porous carbon nanofiber/sulfur cathodes with exceptional high-rate performance

Zheng-Long Xu[1,2], Jian-Qiu Huang[1], Woon Gie Chong[1], Xianying Qin[1], Xiangyu Wang[1], Limin Zhou[2] and Jang-Kyo Kim[1,]*

Dr. Z.L. Xu, J. Q. Huang, W. G. Chong, Dr. X. Qin, X. Wang, Prof. L. Zhou, Prof. J.K. Kim
[1]Department of Mechanical and Aerospace Engineering, The Hong Kong University of Science and Technology, Clear Water Bay, Hong Kong, China
E-mail: mejkkim@ust.hk
[2]Department of Mechanical Engineering, The Hong Kong Polytechnic University, Hung Hom, Kowloon, Hong Kong, China.

Keywords: porous carbon nanofibers, high-rate, lithium-sulfur batteries, volume expansion, *in-situ* TEM

Although lithium sulfur batteries (LSBs) have attracted much interest owing to their high energy densities, synthesis of high-rate cathodes and understanding their volume expansion behavior still remain challenging. Herein, electrospinning is used to prepare porous carbon nanofiber (PCNF) hosts, where both the pore volume and surface area are tailored by optimizing the sacrificial agent content and the activation temperature. Benefiting from the ameliorating functional features of high electrical conductivity, large pore volume and Li ion permselective micropores, the PCNF/A550/S electrode activated at 550 °C exhibits a high sulfur loading of 71 wt.%, a high capacity of 945 mAh g^{-1} at 1C and excellent high-rate capability. The *in-situ* TEM examination reveals that the lithiation product, Li_2S, is contained within the electrode with only ~35 % volume expansion and the carbon host remains intact without fracture. In contrast, the PCNF/A750/S electrode with damaged carbon spheres exhibits sulfur sublimation, a larger volume expansion of over 61 % and overflowing of Li_2S, a testament to its poor cyclic stability. These findings provide, for the first time, a new insight into the correlation between volume expansion and electrochemical performance of the electrode, offering a potential design strategy to synthesize high-rate and stable LSB cathodes.

1. Introduction

The ever-growing portable electronics markets demand energy storage systems with high energy/power densities, long cyclic performance, low costs and eco-friendly characteristics. Among many different electrochemical energy storage devices, lithium ion batteries (LIBs) have dominated the market for over two decades due to their long cyclic life and affordability.[1] To satisfy the emerging applications in next-generation electric vehicles (EVs) and large scale electrical grids requiring higher energy densities, the current LIBs using graphite as anode and lithium metal oxides as cathode are far from sufficient. Lithium sulfur batteries (LSBs) are considered one of the most promising alternatives to LIBs because sulfur can offer a high specific capacity of 1675 mAh g^{-1}, a moderate working potential of about 2.1 V and a remarkable theoretical energy density of 2567 Wh kg^{-1}. Moreover, sulfur is abundant on earth and environmentally benign.[2,3] Despite these attractive characteristics, several challenges have hindered their practical applications.[4] For example, (i) the poor electrical conductivities of sulfur (5×10^{-30} S cm^{-1}), polysulfides and the resultant Li_2S lead to low utilization of active materials especially at high rates; (ii) the high solubility and severe shuttling effect of intermediate polysulfide products cause poor Coulombic efficiencies and fast capacity degradation; (iii) large volume expansion of 80 % occurs during lithiation due to the different densities between sulfur (2.07 g cm^{-3}) and Li_2S (1.66 g cm^{-3}), leading to structural instability of the electrodes.

In order to overcome the above obstacles, many approaches have been devised, such as developing multifunctional hosts, modifying the electrolyte and inserting polysulfide-blocking interlayers.[5-8] Among them, confining sulfur and polysulfides within the physically and chemically stable, conductive carbon hosts is one of the most effective strategies to prevent polysulfide shuttling while accommodating the volume expansion and offering a high conductivity to the electrode. In this respect, various porous carbon materials, including graphene (G), carbon nanotubes (CNTs), carbon nanofibers (CNFs) and carbon spheres (CSs),

have been extensively investigated to synthesize sulfur/carbon composites with improved electrochemical performance.[9, 10] In particular, CNFs with high aspect ratios, tunable porosities and electrical conductivities, facile synthesis processes and feasibility for mass production, provides new opportunities to prepare CNF/sulfur composites with desirable structures and properties.[11-22] For example, freestanding and flexible CNF/S electrodes were synthesized by incorporating sulfur in porous CNF films.[15, 16] Multichannel CNF/S cathodes encapsulated with pie-like graphene have been developed for LSBs with high areal energy densities.[17] Polysulfide absorbers, like nitrogen-doping groups,[18, 19] MnO_2,[20] TiO_2,[21] polyvinyl pyrrolidone (PVP),[22] were incorporated into the electrodes to immobilize polysulfides for enhanced cyclic stability. However, when designing high-power LSBs, the CNF/S cathodes exhibiting high capacities at low rates usually encounter sharp decay in capacity at high rates.[15-19] For example, N-doped porous CNF/S electrodes delivered an exceptional capacity of 1173 mAh g^{-1} at 0.2 C (where 1 C = 1675 mA g^{-1}), but they retained only 400 mAh g^{-1} at 2 C.[19] This means that designing CNF/sulfur electrodes having acceptable high-rate capabilities still remains a big challenge.

When carbon materials are selected for high-rate and stable LSB cathodes, the following characteristics are commonly sought: [23] (i) excellent electrical conductivities for fast electron transport; (ii) hierarchical nanopores as effective ion diffusion channels and paths for electrolyte penetration; (iii) excellent mechanical stability/flexibility to accommodate the volume expansion and mitigate polysulfide diffusion. Several novel CNT/S and G/S composites have recently been reported with excellent high-rate performance.[24-28] In particular, the electrodes prepared from holey CNT/S covered with ZrO_2 (h-CNT/S/ZrO_2) displayed impressive capacities ranging 900-1000 mAh g^{-1} at high rates of 4-8 C. Without exception, the extremely high electrical conductivity of CNTs and the curtailed Li ion diffusion paths through the activated holes on CNT walls enabled ultrafast charge/discharge cycles.[24] However, the delicate, complex structure of h-CNT/S/ZrO_2 means complicated

synthesis processes using expensive CNTs, which not only makes large-scale production difficult but also discounts the low-cost advantage of LSBs. More importantly, the low sulfur content of 45 wt.% also makes it difficult to achieve competitive volumetric capacities required for real-world applications.

When the carbon/sulfur cathode is designed to contain a high sulfur content, one should take into account the impact of volume expansion because most of the pores are filled with sulfur particles leaving only little empty space to accommodate the volume expansion of sulfur. It has long been assumed that the large volume expansion of active material would cause sulfur particle to fracture, damage the carbon host and loosen the electrical contact between sulfur and carbon,[4] similar to what has been experienced with Si anodes in LIBs.[29, 30] However, neither direct evidence to confirm the above assumption nor any indication for a correlation between the volume expansion of the structure and electrochemical properties of LSBs has thus far been reported.

To address the above challenging issues, this work is dedicated to developing hierarchical porous carbon nanofiber/sulfur (PCNF/S) composites for advanced cathodes with a high sulfur loading and a high-rate capability. We achieved excellent electrochemical performance due to their unique structural and functional features that previously-reported porous CNF/S composite electrodes lacked.[15-22] *In-situ* TEM was then used to examine in real time the lithiation behavior of porous CNF/S electrodes so as to provide solid evidence for the correlation between their electrochemical performance and volume expansion.

2. Results and discussion

2.1 Morphologies and structures of PCNF/S electrode materials

The overall synthesis procedure of PCNF/S composites involved three steps, as schematically shown in **Figure 1**. They include (i) carbonization of electrospun PAN/iron(III) $(acac)_3$ neat fibers, (ii) acid etching and chemical activation to obtain PCNFs and (iii) the infiltration of molten sulfur into the PCNFs by melt diffusion. It is demonstrated previously that iron

precursors catalyzed the formation of graphitic carbon layers during the low temperature carbonization process by forming Fe_3C particles.[31] When the catalytic Fe_3C particles were etched off by nitric acid, hollow graphitic carbon spheres of a few tens of nanometers in diameter were created in the CNF matrix (**Figures 2**a-b). The hollow internal space within the tiny graphitic carbon spheres served as sulfur container, while the conductive graphitic carbon layers functioned as fast paths for electron transfer, both of which are important in delivering high capacities and high rate performance of the electrodes.

To optimize the pore volume and surface area in PCNFs, we altered the iron precursor contents and obtained four different groups of porous CNFs designated as PCNF-0.25, PCNF-0.5, PCNF-1 and PCNF-2 depending on the mass ratio of iron(III)$(acac)_3$:PAN. The iron(III)$(acac)_3$ content could not be further increased because the viscosity of polymer precursor became too low to produce fibers by electrospinning if the weight ratio was higher than 2.[11, 31] Figure 2c shows the N_2 adsorption/desorption isotherms of various porous CNFs, which belonged to type IV with a dominant hysteresis loop at P/P_o between 0.4 and 1, implying the presence of mesopores. **Table S1** summarizes the pore volumes, surface areas and electrical conductivities of the four different porous CNFs, noting interesting results, as follows. Both the pore volume and specific surface area of porous CNFs consistently augmented with increasing iron precursor contents, which is beneficial for a higher sulfur loading. Porous carbons with a higher pore volume favored sulfur utilization at a high sulfur loading,[32] which is also verified by the superior cyclic capacities of the PCNF-2/S cathode, as shown in **Figure S1**. Therefore, the PCNF-2 fibers with the highest pore volume and largest surface area were chosen for the following experiments and simply designated as PCNF.

The electrical conductivities of almost all PCNFs were on the order of 10^{-2} S cm^{-1}, which is three orders of magnitude higher than 10^{-5} S cm^{-1} for the neat CNF films,[31] signifying the contribution from the graphitic carbon layers (Figures 2b and e). Apart from the high

electrical conductivities and large pore volumes, fast charge transfer by efficient access to the active sites by Li ions is another critical criterion for high-rate rechargeable batteries. Thus, the hollow graphitic carbon spheres were subjected to chemical activation in order to increase the Li ion diffusion channels while simultaneously constraining the polysulfide dissolution and maintaining the structural stability. Chemical activation with KOH has been widely studied to prepare porous carbons because of its low cost and the feasibility of large-scale production.[15-16, 33] The mechanisms of KOH activation are still under investigation and are generally depicted as 6 KOH + C ↔ 3 H_2 + 2 K_2CO_3, followed by the decomposition of K_2CO_3 and/or the reaction of $K/K_2O/CO_2$ with carbon.[33] The etching reaction creates pores on the carbon surface with pore size and specific surface area roughly controlled by activation temperature. Since the activation by KOH is less effective at temperatures lower than 500 °C,[33-35] the PCNFs were activated between 550 and 750 °C, the products of which were designated as PCNF/A550, PCNF/A650 and PCNF/A750, respectively. To ensure uniform distribution of KOH on the surface of graphitic carbon (**Figure S2**), PCNFs were soaked in KOH aqueous solution followed by drying and activation, which is different from the previous studies[34-35] involving direct mixture of KOH and porous carbon powders.

Figure 2d presents the microstructure of PCNF/A550 fibers with a diameter of ~200 nm, which comprised interconnected hollow graphitic carbon spheres, similar to the pristine PCNF in Figure 2a. The HRTEM images of an individual carbon sphere show abundant defects in a graphitic carbon wall of ~3 nm in thickness (Figure 2e), implying successful creation of micropores by chemical activation.[13, 36] When the activation temperature was increased to 750 °C, the PCNF/A750 fiber presents wedge-shaped pits on the surface of graphitic carbon or open porous structures as marked by the blue arrows in Figures 2g-h. The corresponding N_2 adsorption/desorption isotherms and pore size distributions curves are shown in Figures 2i-j. The surface areas (in m^2 g^{-1}) and pore volumes (in cm^3 g^{-1}) of PCNF/A550, PCNF/A650 and PCNF/A750 were 893.1/0.81, 993.1/0.82 and 1277.3/0.86,

respectively, which are much larger than the matching values 509/0.78 for the neat PCNFs before activation, suggesting the creation of large amounts of new pores by chemical activation. In particular, the isotherm of PCNF/A550 showed a type I/IV with a high adsorption volume at relative pressures, P/P_o, below 0.1, and a hysteresis loop at P/P_o between 0.4 and 1, signifying the presence of micro-mesopores.[34-35] This observation is supported by the pore size distribution in Figure 2j, where PCNF/A550 had dominant micropores at 0.54, 0.86 and 1.26 nm along with meso-macropores in the range of 10-75 nm. Meso-macropores were also observed in other fibers, PCNF, PCNF/A650 and PCNF/A750, representing those left after etching of Fe_3C particles. In addition, a prominent peak at ~8 nm in PCNF/A750 and another sharp peak at ~2.8 nm in PCNF/A650 were observed, possibly referring to those created on graphitic carbon walls. In brief, it can be said that micropores (< 2nm in PCNF/A550), small mesopores (~2.8 nm in PCNF/A650) and mid-sized mesopores (~8 nm in PCNF/A750) were introduced to the PCNFs by tailoring the activation temperature. It is noted that the electrical conductivity of PCNFs was slightly decreased by activation, but the values listed in Table S1 for activated PCNFs were still much higher than ~10^{-5} S cm^{-1} of the neat CNF.[31]

The PCNFs were integrated with sulfur by melt-diffusion.[17-22] **Figures 3**a-d display TEM images and the corresponding elemental maps of a PCNF/A550/S fiber which contained sulfur in the hollow carbon spheres. The small black particles in PCNF/A550/S may be attributed to a small amount of residual Fe_3C, in agreement with our previous work.[31] The energy dispersive spectroscopy (EDS) elemental maps confirmed that (i) sulfur were uniformly integrated with the PCNF/A550 host and (ii) the PCNF/A550/S fiber contained a significant amount of nitrogen (Figures 3d). To verify whether sulfur was successfully encapsulated within the PCNF/A550 host, a HRTEM image and EDS elemental maps of an individual sulfur/carbon sphere are presented in Figures 3e-g. The solid carbon/sulfur sphere presented uniform distributions of both sulfur and carbon elements. The sulfur contents of

various porous CNF/S composites were measured by TGA (**Figure S3**) and are given in Table S1. To analysize N-doping, the N1s peak in general XPS spectrum (Figure S3) was deconvoluted into pyrrolic N (at 398.3 eV), pyridinic N (at 400.0 eV) and graphitic N (at 404.5 eV) (Figure 3h) and the N content was determined to be 7.5 at.%. The *in-situ* N-doping arose from the inherently high N content of ~26.4 wt.% in PAN precursor. It is proposed previously [7, 18-19] that the N-containing groups immobilized polysulfides diffusion by coordinative interactions with lithium polysulfides to the benefit of enhanced cyclic stability. After the incorporation of sulfur, the electrical conductivities of PCNF/S, PCNF/A550/S, PCNF/A650/S and PCNF/A750/S were measured to be 1.8×10^{-2}, 9.8×10^{-3}, 3.8×10^{-3} and 5.7×10^{-4} S cm^{-1} (Table S1), respectively, which are slightly lower than those of the corresponding porous CNF hosts. [23, 37] However, these values were much higher than ~10^{-5} S cm^{-1} of neat CNFs, indicating the enhanced electrical conductivities of sulfur electrodes.

2.2 Electrochemical performance of PCNF/S electrodes

The cyclic performance of the PCNF/S, PCNF/A550/S, PCNF/A650/S and PCNF/A750/S electrodes measured at 1 C are shown in **Figure 4**. The initial capacities of the four electrodes were 415, 945, 965, 1010 mAh g^{-1}, corresponding to 24.8, 56.4, 57.6 and 60.2 % of the theoretical capacity of 1675 mAh g^{-1} of sulfur cathodes (Figure 4a). These values indicate that (i) the sulfur utilization in the three PCNF/S electrode made from the chemically activated PCNF was much higher than that of the pristine PCNF electrode, due to the increased ion diffusion channels and sulfur/carbon contact areas,[24] and (ii) the initial discharge capacities were higher for the PCNF hosts activated at higher temperatures.[32] Interestingly, the residual specific capacities of these four cathodes after 200 cycles were 486, 765, 562 and 540 mAh g^{-1} with the corresponding capacity retention rates of 117 %, 81 %, 58 % and 53 %, respectively. These values suggest that (i) the PCNF/S with low sulfur utilization may be partially activated during cycles but still presented very low specific capacities; and (ii) the PCNF/A650/S and

PCNF/A750/S electrodes with remarkable initial capacities suffered much faster capacity decay than the PCNF/A550/S electrode, which is also confirmed by the comparison between the 1st and 200th charge/discharge profiles in Figure 4b. It can be concluded that the PCNF/A550/S electrode made from PCNF/A550 with micropores on the carbon layers, a relatively large pore volume and surface area is the optimized choice in this work by providing high sulfur utilization and excellent cyclability at 1 C.

There are several interesting observations from the discharge/charge profiles in Figure 4b, which are explained here. The 1st discharge plateau at ~2.0 V in PCNF/A750/S was lower than those at ~2.1 V for PCNF/A550/S, PCNF/A650/S (Figure 4b) and other sulfur/carbon cathodes.[19, 20] Three following reasons may be responsible: (i) the electrical conductivity of PCNF/A750/S was much lower than those of the other two electrodes (Table S1). (ii) The sulfur content of PCNF/A750/S was the highest among the three electrodes, namely 72.6, 71.0 and 71.3 wt.% for PCNF/A750/S, PCNF/A550/S and PCNF/A650/S, respectively, causing severe polarization to PCNF/A750/S.[19] (iii) The high current density of 1 C during cycles also deteriorated the polarization. To confirm this, the PCNF/A750/S electrode was cycled at 0.1 C (**Figure S4**), displaying a discharge plateau at normally ~2.1 V, similar to other sulfur/carbon cathodes.[19, 20] Another intriguing observation is that the discharge plateau of PCNF/S slightly increased from 1.87 to 1.90 V after 200 cycles, which can be explained by the slow activation of sulfur particles inside the integrated carbon spheres [13, 38] and the rearrangement of reaction products for enhanced contacts with electrolyte [24] during cycles, consistent with the improved cyclic capacities and decreased charge transfer resistance as discussed in the following.

To understand why the PCNF/A550/S electrode exhibited better electrochemical performance than the other three electrodes, *ex situ* electrochemical impedance spectroscopy (EIS) measurements were conducted after the 1st and 200th cycles.[23-25] The Nyquist plots of the four electrodes are shown in Figures 4c-d and the impedance data obtained from the

equivalent circuit are listed in **Table S2**. R_0, R_{ct1} and R_{ct2} in the equivalent circuit attribute to the resistance of electrolyte and cell components, the resistance between electrolyte and electrode interface and the resistance to charge transfer, respectively. CPE and W_o denote the constant phase element and the Warburg resistance, respectively.[24-26] For the 1st cycled cells, the resistances, R_{ct1} and R_{ct2}, measured for PCNF/A550/S (48.3/33.8 Ω), PCNF/A650/S (39.6/27.5 Ω) and PCNF/A750/S (12.5/12.0 Ω) were much smaller than 75.9/41.8 Ω for PCNF/S, suggesting that these resistances were significantly reduced by chemical activation of PCNFs. The Li ion diffusion coefficients, D, were calculated from the Warburg region using the equation (S2), see Supporting Information for details.[36] $D = 1.7 \times 10^{-12}$ cm^2 s^{-1} of PCNF/A550/S was much higher than 7.2×10^{-13} cm^2 s^{-1} for PCNF/S. Both the impedance and diffusion coefficient data indicate promoted reaction kinetics of the cathodes made from the activated PCNFs, leading to enhanced initial discharge capacities. It is noted that the PCNF/A750/S cathode with a low EIS impedance delivered a high polarization (Figure 4b), which may be attributed to the poor electrical conductivity of the PCNF/A750/S composite.[24, 39-40] After 200 cycles, the PCNF/A550/S electrode presented much reduced resistances, R_{ct1}/R_{ct2} (10.7/10.3 Ω), together with a high Li diffusion coefficient of 2.9×10^{-12} cm^2 s^{-1}, a reflection of enhanced reaction kinetics. In contrast, both the PCNF/A750/S and PCNF/A650/S electrodes had lower ion diffusion coefficients of 4.9×10^{-13} and 1.3×10^{-12} cm^2 s^{-1}, respectively. These findings imply severe dissolution of polysulfides and the deposition of insulating Li_2S/Li_2S_2 layers on the surface of these electrodes. They were also reflected by the fast capacity degradation, the shortened discharge plateau at ~2.0 V and the upshift of charge plateau in the 200th discharge/charge profiles (Figure 4b). Therefore, it can be said that the activated micropores on PCNF/A550 promoted reaction kinetics and facilitated immobilization of polysulfides better than the mesopores on PCNF/A650 and PCNF/A750.[41, 42] It should be noted that the resistances, R_{ct1} and R_{ct2}, of all electrode

materials decreased by large margins after 200 cycles,[24, 43-44] possibly due to the better access of electrolyte to active materials by structural re-arrangement and formation of liquid polysulfide, which is consistent with the upshift of discharge voltage in the CV curves (**Figure S5**).[24]

The rate performance of the PCNF/A550/S electrode with a relatively high sulfur mass loading of 1.5 mg cm^{-2} measured at current rates ranging from 0.1 to 2.0 C is presented in **Figure 5**a. The reversible capacity became stabilized at 1025 mAh g^{-1} when tested at an initial 0.1 C, and gradually decreased to 906, 799, 742 and 697 mAh g^{-1} at 0.3, 1.0, 1.5 and 2.0 C, respectively. When the rate was reverted to 0.1 C, the reversible capacity was recovered to 910 mAh g^{-1} and maintained stable, verifying that the electrode remained structurally stable even after charge/discharge cycles at high rates. The corresponding charge/discharge profiles are shown in Figure S5. These high-rate capacities are compared with similar CNF/sulfur composite electrodes reported previously, as shown in Figure 5b. The capacity retention of the PCNF/A550/S electrode for a current density increase from 0.1 to 2 C was 68 %, which is much higher than the corresponding values of 44 % for CNF/S,[13] 28 % for G-PCNF/S, [17] and 59 % for MnO_2-CNF/S for a current density change from 0.05 to 1 C,[20] indicating outstanding high-rate capability of the current cathode. This can be ascribed to the ameliorating structural features of PCNF/A550/S composites with favorable properties. (i) The degree of graphitization and electrical conductivity of PCNF/A550/S were much higher than CNF/sulfur cathodes comprising amorphous carbon hosts [12, 15-18] or/and insulating metal oxides.[20-21] (ii) The abundant micropores created on the surface of graphitic carbon walls provided fast ion diffusion channels and electrolyte infiltration paths. (iii) The micropore-engineered carbon spheres in PCNF/A550 not only maintained structural integrity by accommodating volume expansion of sulfur, but also served as physical barriers to prevent the diffusion of polysulfides, making it possible to retain high capacities during rate cycles.

To further demonstrate the high-rate capability of PCNF/A550/S, the batteries were cycled at extremely high rates of 2.5 and 4 C for 200 cycles as shown in Figure 5c. The reversible capacities obtained at the 200th cycle were 625 and 553 mAh g^{-1} at 2.5 C and 4 C, respectively, with remarkable capacity retention and high Coulombic efficiencies of nearly 100 %. To verify the long-term stability of PCNF/A550/S, the batteries were cycled at 1.5 C for 500 cycles (Figure S5). The PCNF/A550/S cathode delivered excellent capacities of 766 and 509 mAh g^{-1} at the 1st and 500th cycle, respectively, giving rise to a low capacity decay rate of 0.067 % per cycle. This value is much lower than those for many reported cathodes, i.e. 0.17 % for graphene oxide/CNT interlayer,[8] 0.12 % for G-CNT/S [23] and 0.11 % for h-CNT/S/ZrO_2.[24] **Table S3** summarizes the cyclic capacities of various CNF/sulfur cathodes, showing that the current electrode with a high sulfur loading of 71 wt.% offered one of the best high-rate performance to date.

2.3 Lithiation processes in PCNF/S electrodes by *in situ* TEM examination

In addition to the excellent electrochemical performance obtained for the PCNF/S electrodes, equally important is to understand the local reaction mechanisms taking place during lithiation/delithiation on the nanoscale, which can not only provide insights into the degradation mechanisms but also offer fundamental guidance towards designing better LSBs.[45, 46] We carried out *in-situ* TEM examination to study the lithiation process with a special emphasis on quantitatively measuring the volume expansion of the electrodes, especially using the representative PCNF/A550/S and PCNF/A750/S electrodes.

Figure 6a presents a schematic of the experimental setup where a potential of -2 V vs Li/Li$^+$ was applied to drive lithiation when a physical contact was confirmed between the Li/Li_2O reference electrode and the porous CNF/S working electrode.[29, 47] The gradual volume expansion due to lithiation of the PCNF/A550/S electrode was recorded in **Movie S1**, from which the captured images taken of the initial and fully lithiated stages are shown in Figures 6b-d. It is worth noting that the lithiation process was uniform over the whole circular cross-

section. The selected area electron diffraction (SAED) patterns indicate that the amorphous sulfur (inset of Figure 6b) in the pristine PCNF/A550/S fiber was transferred to crystalline Li_2S (inset Figure 6c) after lithiation.[46] **Figure S6** shows a higher resolution TEM image of the lithiated region and the corresponding SAED pattern, displaying Li_2S grains of about 10-20 nm in size.[45] To measure the volume expansion, a ~450 nm long circular truncated cone with diameters of ~171 nm and ~224 nm on the top and bottom areas, respectively, were selected as indicated by the prominent markers and black arrows (Figure 6b). After full lithiation, the two positioning arrows placed at the markers remained unexpanded, while the diameters expanded to ~210 and ~251 nm, respectively, giving a volume expansion of ~35 %. This value is much smaller than the theoretical 80 % for sulfur, due to the below reasons. (i) The graphitic carbon layers significantly limited the expansion of lithium sulfide during lithiation. The lithiated PCNF/A550/S presented neither fracture of carbon layers nor overflowing of Li_2S (Figure 6d), indicating successful confinement of Li_2S by the mechanically robust carbon layers. (ii) The PCNF/A550/S electrode had a small amount of pores that accommodated the volume expansion by rearranging reaction products, as mentioned above. (iii) It is also possible that sulfur and Li_2S were evaporated under high vacuum and from the irradiation of high energy beam, although the former two reasons played more important roles. The significantly low volume expansion and excellent structural stability of the PCNF/A550/S electrode provided solid evidence for its excellent cyclic stability in real batteries.

In comparison to the stable PCNF/A550/S, the *in-situ* TEM examination (Figures 6e-g) of PCNF/A750/S presented three major differences: namely, (i) sublimation of sulfur; (ii) larger volume expansion; and (iii) overflowing of Li_2S. Figure 6e shows the TEM image of a pristine PCNF/A750/S fiber with a light-colored sheath and a dark-colored core, which is different from the uniform color of PCNF/A550/S (Figure 6b). The light-colored sheath is the consequence of the sublimation of sulfur from the carbon host.[48] The different degrees of

stability of sulfur in the two materials, PCNF/A550/S and PCNF/A750/S, should be directly related to differing microstructures of their PCNF hosts. PCNF/A750 possessed mid-sized mesopores of ~8 nm in diameter while PCNF/A550 had micropores smaller than 2 nm on the carbon walls. When the pore size was too large or pores were damaged (Figure 2h-g), the carbon shell was not able to protect the exposed sulfur from heating by electron beams, leading to the evaporation of sulfur. In contrast, PCNF/A550 with integrated carbon walls helped dissipate the heat to retain the internal sulfur.[48, 49] In addition, the vapor pressure goes down when a substance is confined within a porous material. However, the larger the pore is, the higher the vapor pressure would be, according to the Barrett-Joyner-Halenda theory.[50] It follows that when the vapor pressure was higher than the vacuum of the TEM chamber (~10^{-5} Pa), the sulfur in the porous CNF/S would be sublimed off. It was reported that hollow carbon spheres with pore sizes larger than 2.8 nm in sheath failed to prevent sulfur sublimation in STEM/TEM.[48] Thus, it can be expected that PCNF/A750 with pores of ~8 nm on carbon walls encouraged the sublimation of sulfur under TEM, while PCNF/A550 having micropores did not. One may argue that PCNF/A750/S was not filled with sulfur before TEM experiments, suspecting the validity of the above explanation. To verify sulfur was indeed filled before revealing the sublimation behavior, we purposely applied a flexible poly (3,4-ethylenedioxythiophene) (PEDOT) coating because the polymer coating could effectively prevent heating and sublimation of sulfur during the TEM experiments.[48, 51] As shown in **Figure S7**, the polymer-coated PCNF/A750/S was filled with sulfur, indicating sublimation of sulfur in the pristine PCNF/A750/S while taking TEM images. Therefore, we can unambiguously conclude that the sulfur in PCNF/A750/S sublimated during TEM experiments, which is not observed in PCNF/A550/S containing micropores. To alleviate further sublimation of sulfur in PCNF/A750/S, we conducted the *in-situ* lithiation of the electrode without illuminating electron beams except for very quick imaging once every five min.[52]

The volume expansion of PCNF/A750/S was calculated from the changes in diameter and length, giving ~61 % (Figure 6e-f). This value is close to the theoretical value of 80 % and is much larger than ~35 % of PCNF/A550/S. In view of the sublimation of sulfur in the pristine fiber, the real volume expansion of PCNF/A750/S can be even larger than 61 %. The high magnification TEM image (Figure 6g) indicates that the lithiation product, Li_2S, spilled over the carbon spheres as a result of large volume expansion of the PCNF/A750/S electrode. These findings are related to the pore size and mechanical properties of the carbon spheres in the PCNF/A750 host. During the *in-situ* TEM lithiation, the Li_2S phase was formed directly without generating long-chain lithium polysulfides unlike in real batteries.[45, 46] The molecular size of Li_2S was ~ 0.5 nm,[53] which is far smaller than the mesopores of ~8 nm in diameter in PCNF/A750, thus their graphitic carbon spheres could not prevent the overflowing of lithiation products. In contrast, the carbon spheres in PCNF/A550 containing micropores of ~0.54 nm in diameter functioned as the physical barriers to contain lithium sulfides.[41, 54] In addition, the graphitic carbon spheres in PCNF/A750 were severely damaged by high-temperature activation (Figures 2g-h), which impaired their role as the buffer against the volume expansion of sulfur.[55] To evaluate whether the carbon spheres in the PCNF/A750 host sustained the swelling of sulfur, the volume expansion of the dark-colored core of PCNF/A750/S was measured based on the change in diameter after full lithiation from ~158 to ~210 nm and the change in length from ~590 to ~663 mm. The expansion was ~98 % which we assume is more accurate than the aforementioned total volume expansion of ~61 % because the core area is less affected by TEM environment than the sheath. This value is also much larger than ~35 % for PCNF/A550/S, meaning that the damaged carbon spheres were not able to effectively suppress the expansion of sulfur in PCNF/A750/S. It is also noted that ~98 % is larger than the theoretical value of 80 %, probably due to the spread of lithium sulfides in the PCNF host. In summary, it can be said that the PCNF/A750/S electrode with

mid-sized mesopores (~8 nm) and poor mechanical stability can neither effectively confine lithium sulfides nor accommodate the volume expansion during lithiation, offering a testament to its poor cyclic stability and severe polysulfide diffusion in practical batteries.

It should be noted that the electrode/electrolyte interface of the *in-situ* TEM nanocell is not identical to that in practical batteries with liquid electrolyte, and the TEM environment with electron beams under high vacuum may also inadvertently affect the lithiation behavior of PCNF/S electrodes. Yet, we believe that our quantitative analysis of volume expansion of PCNF/S cathodes by *in-situ* TEM study can provide invaluable insights into the failure mechanisms and structural evolution of porous CNF/sulfur cathodes. To compensate the shortcoming of *in-situ* TEM in estimating the immobilization of polysulfides by porous CNF/sulfur cathodes in liquid electrolyte, we studied the *in-situ* electrochemical behaviors of PCNF/A550/S and PCNF/A750/S in transparent LSBs **(Figure S8)**.[56] Interestingly, the colorless electrolyte around the PCNF/A550/S cathode kept almost unchanged after discharging, in sharp contrast to the yellow electrolyte in the PCNF/A750/S battery. This finding offered solid evidence for structural stability and effective confinement of polysulfides in PCNF/A550/S cathodes, which is highly consistent with the *in-situ* TEM observations and electrochemical performance.

By combining the *in-situ* results with the microstructures and electrochemical properties of various PCNF/S electrodes, this work elucidated several important guidelines to design PCNFs for high-rate and stable LSBs, as follows. (i) The PCNFs with a high electrical conductivity, a large pore volume, a large surface area, activated pores on carbon walls are beneficial to high-rate capability at a high sulfur loading. (ii) One should keep in mind that the nanosized pores created for fast ion diffusion may also promote the dissolution of polysulfides and weaken the mechanical stability of carbon host, which are unfavorable for cyclic stability. (iii) Micropores created on carbon walls are more favorable than mesopores, which can not only provide ion transport pathways but also constrain the volume expansion and immobilize

lithium sulfides. (iv) The volume expansion and overflowing of lithiation products in PCNF/S cathodes are closely related to the microstructure and mechanical stability of carbon hosts.

3. Conclusion

In summary, we have prepared porous CNF/S composites as high-rate LSB cathodes in a sequential process of scalable electrospinning, chemical activation and melt diffusion. The pore volume, surface area and post-activated pore distribution of CNF hosts were rationally tuned by adjusting the content of sacrificial agent and the activation temperature. An optimal condition was identified to synthesize PCNF/A550 possessing ameliorating functional features of high electrical conductivity, large pore volume and surface area, as well as abundant micropores. The PCNF/A550/S electrode after infiltration of a high sulfur loading of 71 wt.% delivered a high initial discharge capacity of 945 mAh g^{-1} at 1 C with excellent cyclicality and high-rate capacities at 2.5 and 4.0 C for 200 cycles. The *in-situ* TEM technique was used to obtain insightful understanding of the correlation between the evolution of local structures on a nanoscale and the electrochemical performance on a macroscale. It is revealed that the PCNF/A550/S electrode not only confined the lithiation product of Li_2S with a low volume expansion of ~35 %, but also maintained structural stability without fracture of the carbon host. In contrast, the PCNF/A750/S electrode with damaged/open carbon spheres presented sublimation of sulfur, a larger volume expansion of over 61 % and overflowing of Li_2S due to structural instability, consistent with its fast capacity degradation and polysulfide diffusion in real batteries. This work can offer both a potential strategy to prepare high-rate sulfur/CNF cathodes by rationally designing pores in CNFs and, for the first time, a new insight into volume expansion of the electrode by *in-situ* TEM examination.

4. Experimental section

Preparation of porous CNF/S composites: The electrospinning precursor was prepared by dissolving 0.5 g polyacrylonitrile (PAN) in 20 ml N,N-dimethylformamide (DMF) solvent

and magnetically stirring for 8 h at 80 °C. 1.0 g iron (III) acetylacetonate was added to the above solution, which was stirred for 8 h. The polymer mixture was electrospun on an electrospinner (KATO Tech. Co., Japan) at 18 kV and the distance between the needle and the collector was maintained at 15 cm. The flow rate of electrospinning and the rotation speed of the drum collector were kept at 1.0 ml h^{-1} and 1.0 m min^{-1}, respectively. The electrospun PAN/iron(III) acetylacetonate films were stabilized at 220 °C for 3 h in an air-circulated oven. Subsequently, the films were carbonized at 650 °C for 0.5 h under N_2 flow at a ramp rate of 5 °C min^{-1} in a tube furnace (Lindberg/Blue, 1700 °C). The resultant CNF films contained Fe_3C nanoparticles which were removed by soaking in fuming HNO_3 for 10 h. CNFs with different porosities were prepared by altering the mass ratios of iron (III) acetylacetonate to PAN when preparing the electrospinning precursor. The porous CNFs were collected by vacuum filtration and soaked in KOH solution at a mass ratio of 1:4. The porous CNF/KOH mixture was then transferred to a tube furnace and heated at 550 °C for 0.5 h at a ramp rate of 2 °C min^{-1}. The resulting product was washed with diluted HCl acid and deionized water to obtain PCNF/A550. The CNF/KOH mixture was also activated at different temperatures. The PCNF/A550 was mixed with sulfur particles at a mass ratio of 1:3, and stirred in CS_2 solution for 0.5 h before drying. The PCNF/A550/S mixture was then placed in a tube furnace under N_2 flow and heated at 155 °C for 12 h to infiltrate molten sulfur within the activated PCNF. The excess sulfur particles on the surface of PCNF/A550/S were removed by heating at 250 °C for 0.5 h. Other porous CNF/S composites were prepared in the same way.

Materials characterization and electrochemical tests: The morphologies were characterized using a scanning electron microscope (SEM, 6700F) and a transmission electron microscope (TEM, JEOL2010). The elemental mapping of porous CNF/S fibers was conducted on an EDS within TEM JEOL2010. The N_2 adsorption/desorption isotherms were obtained at 77 K using an automated adsorption apparatus (Micromeritics, ASAP 2020). The surface area and pore size distribution were determined based on the Brunauer-Emmett-Teller (BET) equation

and the non-localized density functional theory (NLDFT), respectively. The composition of the porous CNF/S composites was evaluated by thermogravimetric analysis (TGA, Q5000) at a heating rate 5 °C min^{-1} in a nitrogen atmosphere.

To measure the electrochemical performance, the cathodes were prepared by mixing the porous CNF/S composite, carbon black and polyvinylidene fluoride (PVDF) binder at a mass ratio of 7:2:1 using N-methyl-2-pyrrolidone (NMP) solvent. The slurry mixture was cast onto an aluminum foil and dried at 80 °C in an air-circulated oven. The cathodes were cut into discs (Φ= 14 mm) with an average sulfur loading of ~1.5 mg cm^{-2}. CR2032 coin cells were assembled using porous CNF/sulfur as the cathode and lithium foil as the anode in an Ar-filled glove box. The 1.0 M lithium bis-trifluoromethane sulfonylimide (LiTFSI) dissolved in 1,3-dioxolane (DOL) and 1,2-dimethoxyethane (DME) (1:1, v:v) with 1 wt.% $LiNO_3$ additive was used as electrolyte with ~20 µl per electrode, and the polyethylene membrane (Celgard 2400) was employed as the separator. The half cells were cycled at different current densities between 1.7 and 2.8 V on a LAND 2001CT battery tester. The cyclic voltammetry (CV) curves were obtained on a CHI660c electrochemical workstation between 1.7 and 2.8 V at a scan rate of 0.1 mV s^{-1}. The EIS was conducted at a constant perturbation amplitude of 5 mV in the frequency range from 10 mHz to 100 kHz (CHI660c electrochemical workstation).

In-situ TEM examination: In-situ experiments were conducted on a JEOL 2010 TEM equipped with a Nanofactory scanning tunneling microscope (STM) holder. The PCNF/S fibers dispersed on a copper rod of 200 µm in diameter were used as the working electrode, while a thin layer of Li metal scratched on the surface of another Cu wire was used as the counter electrode. The STM holder assembled with two electrodes was then transferred into the TEM chamber with an Ar gas flow. During the transfer process, a thin layer of Li_2O was believed to form as a solid electrolyte. A potential of -2 V vs. Li/Li^+ was applied to drive the lithiation reaction in the working electrode when a physical contact between the two electrodes was confirmed.

Supporting Information
Supporting Information is available from the Wiley Online Library or from the author.

Acknowledgements

This project was financially supported by the Research Grants Council (GRF projects 613612 and 16212814) and the Innovation and Technology Commission (ITF project ITS/318/14) of Hong Kong SAR. The authors also appreciate the technical assistance from the Advanced Engineering Materials Facilities (AEMF) and the Materials Characterization and Preparation Facilities (MCPF) at HKUST. Z.L. Xu was partly supported by the SENG PhD Fellowship from the School of Engineering at HKUST.

Received: ((will be filled in by the editorial staff))
Revised: ((will be filled in by the editorial staff))
Published online: ((will be filled in by the editorial staff))

References

[1] M. Armand, J. M. Tarascon, *Nature*, **2008**, *451*, 652.

[2] P. G. Bruce, S. A. Freunberger, L. J. Hardwick, J. M. Tarascon, *Nat. Mater.* **2011**, *11*, 19.

[3] A. Manthiram, S. H. Chung, C. Zu, *Adv. Mater.* **2015**, *27*, 1980.

[4] A. Manthiram, Y. Z. Fu and Y. S Su, *Acc. Chem. Res.* **2013**, *46*, 1125.

[5] Y.X. Yin, S. Xin, Y. G. Guo and L. J. Wan, *Angew. Chem. Int. Ed.* **2013**, *52*, 13186.

[6] A. Rosenman, E. Markevich, G. Salitra, D. Aurbach, A. Garsuch and F. F. Chesneau, *Adv. Energy Mater.* **2015**, 1500212.

[7] J. Q. Huang, B. Zhang, Z. L. Xu, S. Abouali, M. Akbari Garakani, J. Huang, J.K. Kim, *J. Power Sources* **2015**, *285*, 43.

[8] J. Q. Huang, Z. L. Xu, S. Abouali, M. Akabari Garakani, J.K. Kim, *Carbon* **2016**, *99*, 624.

[9] J. Liang, Z. H. Sun, F. Li and H. M. Cheng, *Energy Storage Mater.* **2016**, *2*, 76.

[10] J. G. Wang, K. Xie and B. Wei, *Nano Energy* **2015**, *15*, 413.

[11] B. Zhang, F. Kang, J. M. Tarascon and J. K. Kim, *Prog. Mater. Sci.* **2016**, *76*, 319.

[12] L. Ji, M. Rao, S. Aloni, L. Wang, E. J. Cairns, Y. Zhang, *Energy Environ. Sci.* **2011**, *4*, 5053.

[13] F. Wu, L. Shi, D. Mu, H. Xu, B. Wu, *Carbon* **2015**, *86*, 146.

[14] S. Lu, Y. Cheng, X. Wu and J. Liu, *Nano Lett.* **2013**, *13*, 2485.

[15] L. Zeng, Y. Jiang, J. Xu, M. Wang, W. Li, Y. Yu, *Nanoscale* **2015**, *7*, 10940.

[16] L. Zeng, F. Pan, W. Li, Y. Jiang, X. Zhong, Y. Yu, *Nanoscale* **2014**, *6*, 9579.

[17] Z. Li, J. T. Zhang, Y. M. Chen, J. Li and X. W. Lou, *Nat. Commun.* **2015**, *6*, 8850.

[18] J. Yang, J. Xie, X. Zhou, Y. Zou, J. Tang, S. Wang, F. Chen, L. Wang, *J. Phys. Chem. C* **2014**, *118*, 1800.

[19] W. Zhou, B. Guo, H. Gao and J. B. Goodenough, *Adv. Energy Mater.* **2015**, 1502059.

[20] Z. Li, J. Zhang, X.W. Lou, *Angew. Chem. Int. Ed.* **2015**, *54*, 1286.

[21] Z. Zhang, Q. Li, S. Jiang, K. Zhang, Y. Lai, J. Li, *Chem. Eur. J.* **2015**, *21*, 1343.

[22] G. Zheng, Q. Zhang, J. J. Cha, Y. Yang, W. Li, Z. W. Seh, Y. Cui, *Nano Lett.* **2013**, *13*, 1265.

[23] H. J. Peng, J. Q. Huang, M. Q. Zhao, Q. Zhang, X. B. Cheng, X. Y. Liu, W. Z. Qian and F. Wei, *Adv. Funct. Mater.* **2014**, *24*, 2772.

[24] Y. Zhou, C. Zhou, Q. Li, C. Yan, B. Han, K. Xia, Q. Gao and J. Wu, *Adv. Mater.* **2015**, *27*, 3774.

[25] F. Jin, S. Xiao, L. Lu and Y. Wang, *Nano Lett.* **2016**, *16*, 440.

[26] B. Li, S. Li, J. Liu, B. Wang and S. Yang, *Nano Lett.* **2015**, *15*, 3073.

[27] G. Zhou, S. Pei, L. Li, D. W. Wang, S. Wang, K. Huang, L. C. Yin, F. Li and H. M. Cheng, *Adv. Mater.* **2014**, *26*, 625.

[28] G. Hu, C. Xu, Z. Sun, S. Wang, H. M. Cheng, F. Li and W. Ren, *Adv. Mater.* **2015**, 4765.

[29] Z.L. Xu, K. Cao, S. Abouali, M. A. Garakani, J. Huang, J. Q. Huang, E. K. Heidari, H. Wang and J.K. Kim, *Energy Storage Mater.* **2016**, *3*, 45.

[30] Z.L. Xu, Y. Gang, M. A. Garakani, S. Abouali, J. Q. Huang and J. K. Kim, *J. Mater. Chem. A* **2016**, *4*, 6098.

[31] B. Zhang, Z. L. Xu, Y. B. He, S. Abouali, M. Akabari Garakani, E. K. Heidari, F. Kang, J. K. Kim, *Nano Energy* **2014**, *4*, 88.

[32] R. Sahore, Barnaby D. A. Levin, M. Pan, D. A. Muller, F. J. DiSalvo, E. P. Giannelis, *Adv. Energy Mater.* **2016**, 1600134.

[33] X. Zheng, J. Luo, W. Lv, D. W. Wang, Q. H. Yang, *Adv. Mater.* **2015**, *36*, 5388-5395.

[34] A.J. Romero-Anaya, M. Ouzzine, M. A. Lillo-Rodenas, A. Linares-Solano, *Carbon* **2014**, *68*, 296.

[35] S. Wu, G. Chen, N. Y. Kim, K. Ni, W. Zeng, Y. Zhao, Z. Tao, H. Ji, Z. Lee, Y. Zhu, *Small* **2016**, *12*, 2376.

[36] J. Cui, Z.L. Xu, S. Yao, J. Huang, J. Q. Huang, S. Abouali, M. Akbari Garakani, X. Ning, J.K. Kim, *J. Mater. Chem. A* **2016**, *4*, 10964.

[37] L. Miao, W. Wang, K. Yuan, Y. Yang and A. Wang, *Chem. Comm*. **2014**, *50*, 13231.

[38] B. Li, S. Li, J. Liu, B. Wang, S. Yang, *Nano Lett*. **2015**, *15*, 3073.

[39] S. H. Chung, P. Han, R. Singhal, V. Kalra and A. Manthiram, *Adv. Energy Mater*. **2015**, *5*, 1500738.

[40] Z. Yuan, H. J. Peng, T. Z. Hou, J. Q. Huang, C. M. Chen, D. W. Wang, X. B. Cheng, F. Wei and Q. Zhang, *Nano Lett.* **2016**, *16*, 519.

[41] Z. Li, Y. Jiang, L. Yuan, Z. Yi, C. Wu, Y. Liu, P. Strasser, Y. Huang, *ACS Nano* **2014**, *8*, 9295.

[42] Q. Sun, B. He, X. Q. Zhang, A. H. Lu, *ACS Nano* **2015**, *9*, 8504.

[43] L. Yuan, H. Yuan, X. Qiu, L. Chen, W. Zhu, *J. Power Sources* **2009**, *189*, 1141-1146.

[44] Z. Lyu, D. Xu, L. Yang, R. Che, R. Feng, J. Zhao, Y. Li, Q. Wu, X. Wang, Z. Hu, *Nano Energy* **2015**, *12*, 657.

[45] H. Kim, J. T. Lee, A. Magasinski, K. Zhao, Y. Liu and G. Yushin, *Adv. Energy Mater.* **2015**, 1501306.

[46] Z. Yang, Z. Zhu, J. Ma, D. Xiao, X. Kui, Y. Yao, R. Yu, X. Wei, L. Gu, Y. S. Hu, H. Li and X. Zhang, *Adv. Energy Mater.* **2016**, 1600806.

[47] Z.L. Xu, B. Zhang, Y. Gang, K. Cao, M. Akbari Garakani, S. Abouali, J. Huang, J.Q. Huang, E. Kamali Heidari, H.T. Wang, J.K. Kim. *Energy Storage Mater.* **2015**, *1*, 25.

[48] W. Zhou, C. Wang, Q. Zhang, H. D. Abruna, Y. He, J. Wang, S. X. Mao and X. Xiao, *Adv. Energy Mater.* **2015**, 1401752.

[49] G. He, S. Everts, X. Liang, M. Cuisinier, A. Garsuch, L. F. Nazar, *ACS Nano* **2013**, *12*, 10920.

[50] E. P. Barret, L. G. Joyner, P.P. Halenda, *J. Am. Chem. Soc.* **1951**, *73*, 373.

[51] S. Chen, B. Sun, X. Xie, A. K. Mondal, X. Huang, G. Wang, *Nano Energy* **2015**, *16*, 268.

[52] X. H. Liu, F. Fan, H. Yang, S. Zhang, J.Y. Huang and T. Zhu, *ACS Nano* **2013**, *7*, 1495.

[53] L. C. Yin, J. Liang, G. M. Zhou, F. Li, R. Saito, H. M. Cheng, *Nano Energy* **2016**, *25*, 203.

[54] Z. Li, L. Yuan, Z. Yi, Y. Sun, Y. Liu, Y. Jiang, Y. Shen, Y. Xin, Z. Zhang and Y. Huang, *Adv. Energy Mater.* **2014**, *4*, 1301473.

[55] Z.L. Xu, B. Zhang, Z.Q. Zhou, S. Abouali, M. Akbari Garakani, J. Huang, J. Q. Huang, J. K. Kim, *RSC Adv.* **2014**, *4*, 22359.

[56] Z. A. Ghazi, L. Zhu, H. Wang, A. Naeem, A. M. Khattak, B. Liang, N. A. Khan, Z. Wei, L. Li and Z. Tang, *Adv. Energy Mater.* **2016**, 1601250.

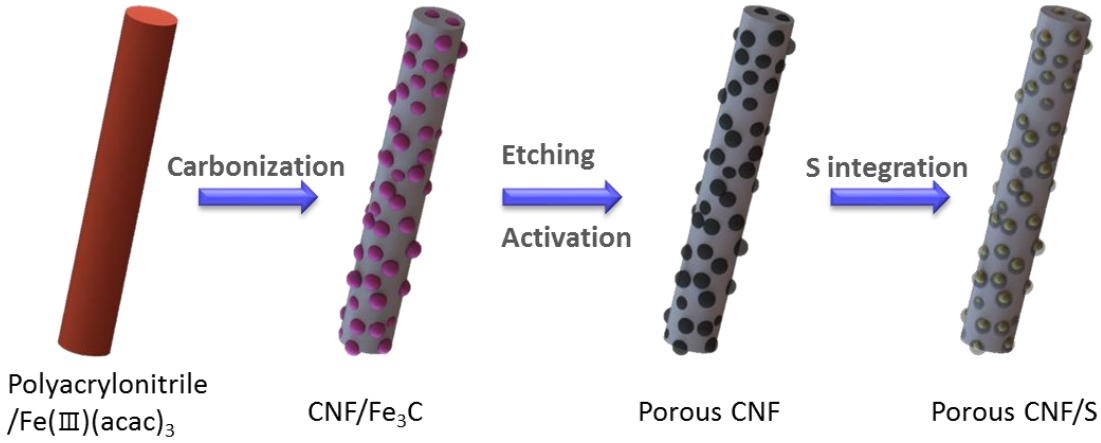

Figure 1. Schematic illustration of the synthesis of porous CNF/S composites: CNF/Fe_3C containing graphitic carbon layer after carbonization; porous CNF after etching Fe_3C and chemical activation; porous CNF/S by infiltrating sulfur.

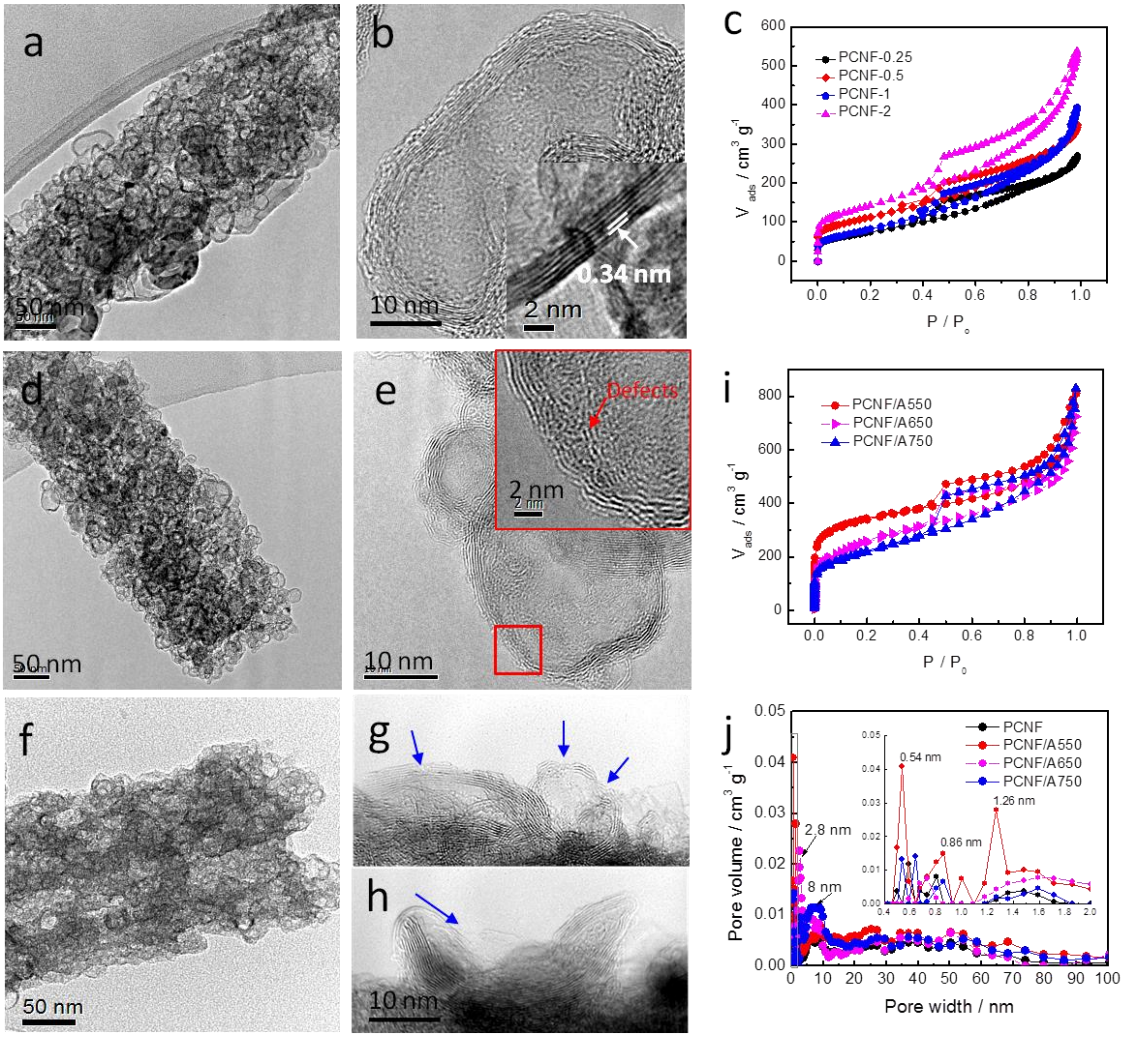

Figure 2. TEM and HRTEM images of (a, b) PCNF, (d, e) PCNF/A550 and (f, g and h) PCNF/A750; N_2 adsorption/desorption isotherms of (c) PCNF-0.25, PCNF-0.5, PCNF-1 and PCNF-2, (i) PCNF/A550, PCNF/A650 and PCNF/A750; (j) pore size distributions of PCNF, PCNF/A550, PCNF/A650 and PCNF/A750.

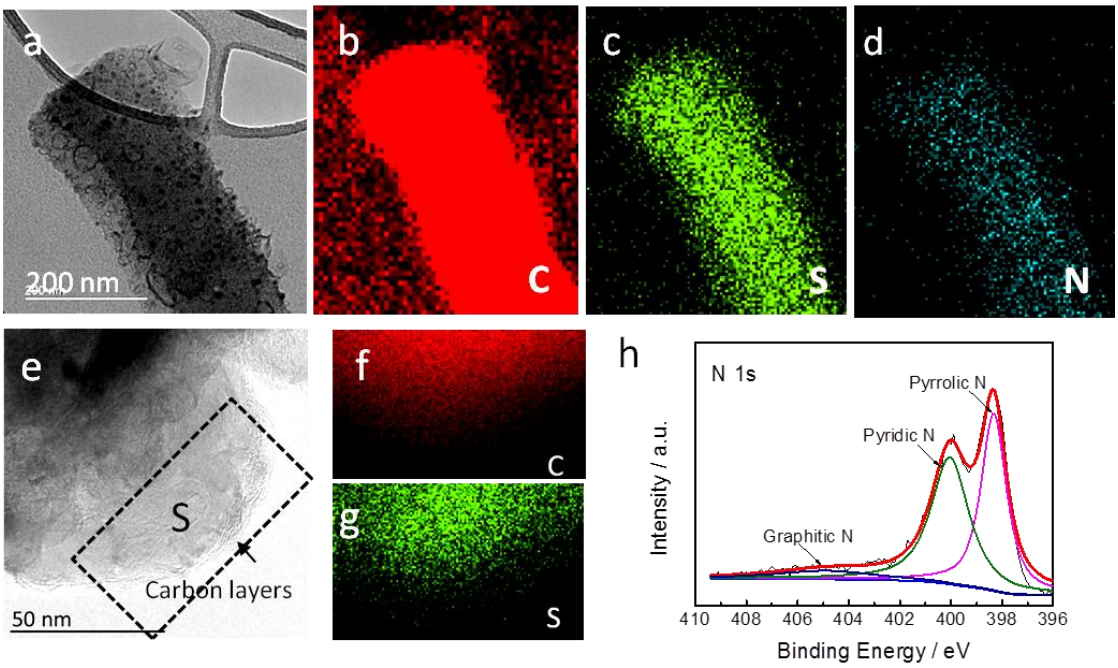

Figure 3. TEM images and corresponding EDS elemental maps of (a-d) a PCNF/A550/S fiber, (e-g) a graphitic carbon sphere filled with sulfur; (h) deconvoluted XPS spectrum of N1s.

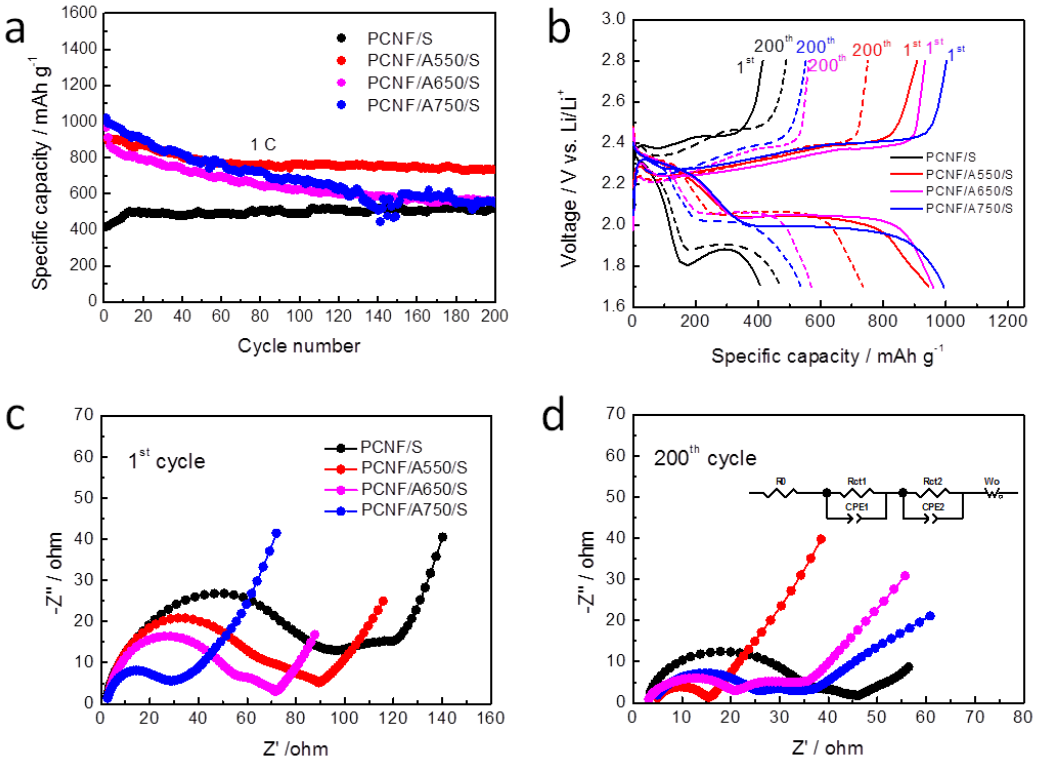

Figure 4. (a) cyclic capacities and (b) discharge/charge profiles of PCNF/S, PCNF/A550/S, PCNF/A650/S and PCNF/A750/S for 200 cycles at 1 C; Nyquist plots of these test cells (c) after the 1st and (d) 200th cycles.

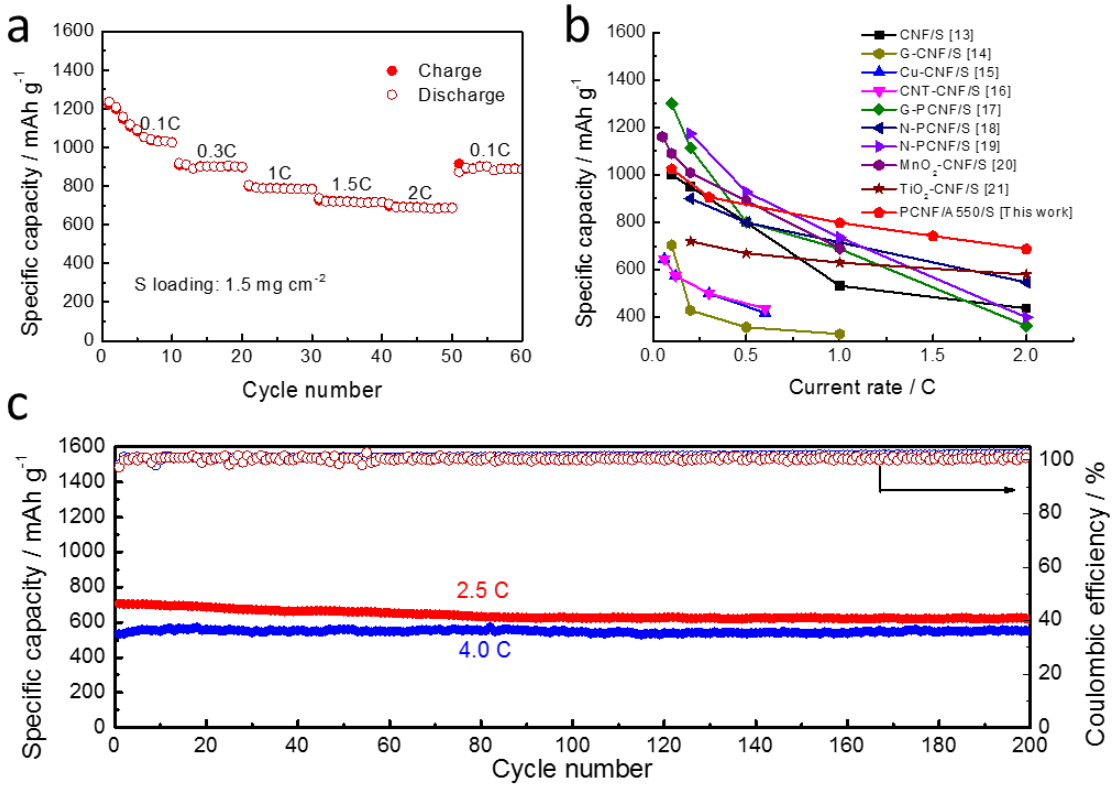

Figure 5. High-rate performance of PCNF/A550/S electrodes: (a) rate capacities from 0.1 C to 2.0 C; (b) comparison of rate capacities between different CNF/sulfur electrodes taken from literature; (c) cyclic capacities and Coulombic efficiencies at 2.5 and 4.0 C for 200 cycles.

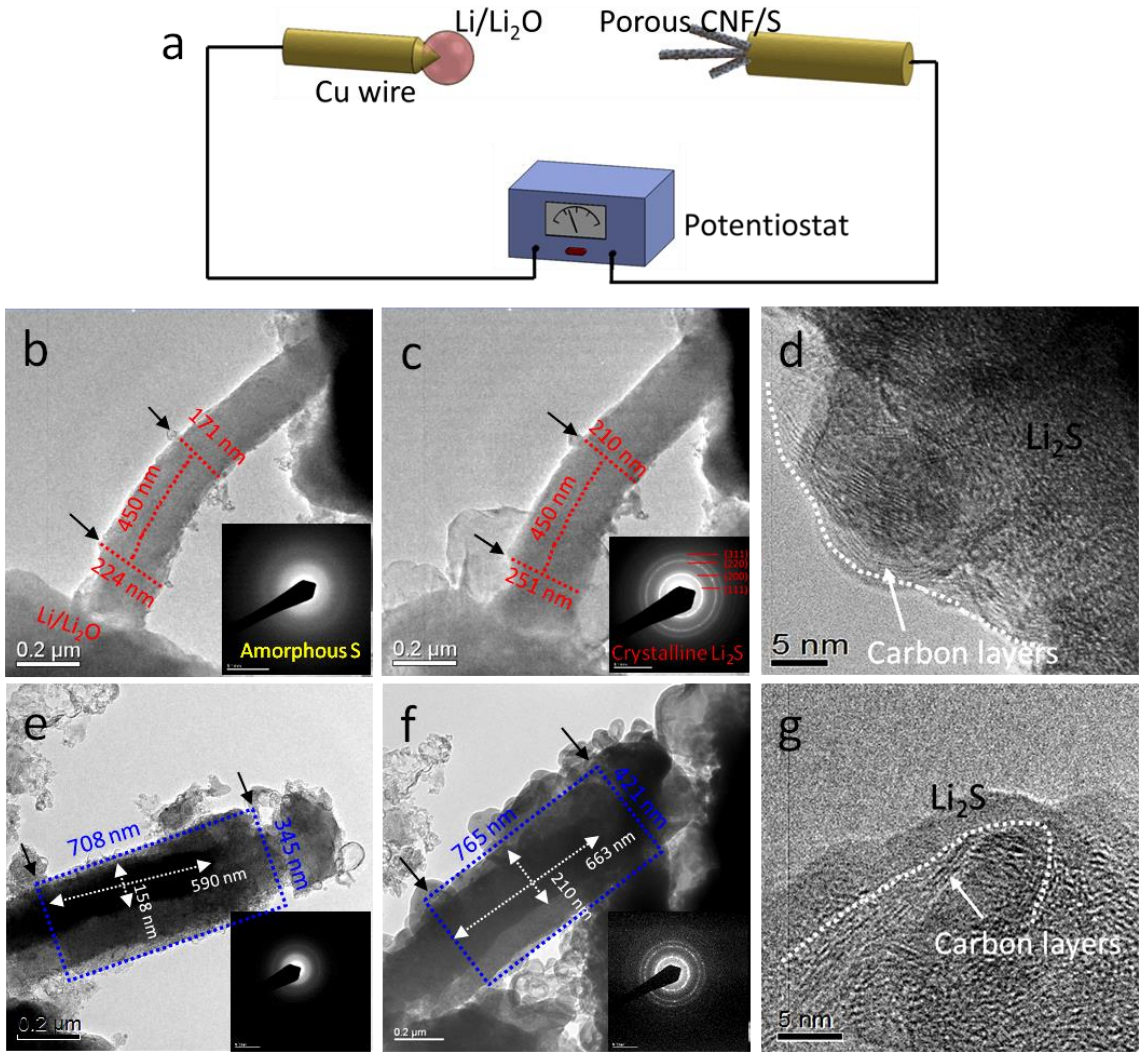

Figure 6. (a) schematic illustration of *in-situ* TEM experiment setup; TEM images and SAED patterns of (b) pristine and (c) fully lithiated PCNF/A550/S; (d) high resolution TEM image of lithiated PCNF/A550/S; TEM images and SAED patterns of (e) pristine and (f) fully lithiated PCNF/A750/S; and (g) high resolution TEM image of lithiated PCNF/A750/S.